Hindawi Publishing Corporation
Shock and Vibration
Volume 2016, Article ID 8403829, 9 pages
http://dx.doi.org/10.1155/2016/8403829

Hindawi

Research Article

Dynamics Analysis on Piezoelectric Laminated Vibrator and Optimization of PZT Position

Caiqi Hu,[1] Xiaoqi Hu,[2] Jing Ji,[1] Jude Liu,[3] and Shengduo Li[1]

[1]*Department of Mechanical and Electrical Engineering, Qingdao Agricultural University, Qingdao 266109, China*
[2]*College of Engineering and Design, Lishui University, Lishui 323000, China*
[3]*Department of Agricultural and Biological Engineering, The Pennsylvania State University, State College, PA 16802, USA*

Correspondence should be addressed to Xiaoqi Hu; huxiaoqi163@163.com

Received 28 June 2015; Revised 21 September 2015; Accepted 30 September 2015

Academic Editor: Francesco Ripamonti

Piezoelectric laminated structure is widely used as actuator's drive part. The different position of PZT on a piezoelectric vibrator causes different incentive effects. Therefore, seeking an optimal PZT position is of great significance to improve actuator's drive forces and electromechanical conversion efficiency. In this research, the optimization of PZT position was studied using the approximate solution of piezoelectric vibrator mode shape with mutation sections. The vibration mode function was expressed as a linear superposition of the admissible function according to Rayleigh Ritz method. Then solving of functional variation was converted into the solving of the coefficient matrix of the admissible function by Hamilton's principle. Through analyzing the forms of admissible functions, the admissible functions that satisfied the boundary conditions of displacement were chosen. For a given vibrator, approximate function for natural frequency and vibration mode was calculated in given admissible functions. Calculated values and experimental results were compared. Results showed that the more items an admissible function sequence had the closer the calculated results were to the experimental values. The errors of calculations were analyzed based on the selection of admissible functions and electromechanical coupling effect. Optimization of PZT position was achieved by analyzing the mode forces of the piezoelectric laminated vibrator.

1. Introduction

Piezoelectric laminated structure is widely used as actuator's drive part as it is well characterized with simple structure, convenient control, quick response, and no electromagnetic pollution [1]. Researchers from all over the world have been involved in the study on theoretical models of such structures extensively [2–5]. Research on how to paste PZT on traveling wave ultrasonic motor indicated that the electromechanical conversion efficiency of piezoelectric ceramics was closely related to the force coefficient which depended on the size and position of the ceramic transducer as well as the mode shape of the stator [6]. Thus, to improve the electromechanical conversion efficiency of the vibrator theoretically, the first thing that must be done is to obtain the vibrator's mode shape and then to determine optimal size and location of a piezoelectric ceramics transducer accordingly. Koplow et al. conducted dynamic analysis on the free vibration of discontinuous beam with one-step change in cross section and predicted the dynamic response of the beam [7]. Sadri et al. established a theoretical model for a thin plate covered with piezoelectric sheets and derived control equations for the plate based on Rayleigh-Ritz method; based on genetic algorithms the optimal placement of piezoelectric actuators was determined, but follow-up experiment verification has not been reported [8]. Bashash et al. divided a variable cross section stepped homogeneous material beam with arbitrary boundary into several segments and built models for them. As a result, characteristic matrix was formed by taking boundary conditions and continuity conditions into consideration [9]. For non-homogeneous piezoelectric beam, however, this approach created a high-order algebraic equation, which is difficult to solve. Crawley and de Luis studied the strain transmitting mechanism from piezoelectric actuator to substructure and conducted researches on PZT optimization position of constant cross section piezoelectric beam and ignored

the influence of PZT on its vibration mode [10]. From the perspective of vibration suppression, Ren and Jiang presented a systematic approach for the free vibration analysis and forced response of the beam bonded with PZT employing the travelling wave method [11]. They found that the PZT bonded position near the fixed end in beam had the powerful actuated capability. However, experiments demonstrated that this conclusion was only applicable to vibration suppression. Cho et al. established an equivalent electric circuit for piezoelectric bimorph beam by using piezoelectric PZT as equivalent to an impedance element [12], and the researches provided the new idea for mathematical model of piezoelectric laminated structure. However, the PZT position optimization was not mentioned. Xu and Zhou presented a two-dimensional analysis for piezoelectric beam with variable thickness under the boundary condition of the simple support [13]. Mao proposed a solution for the problem of finding the shape of piezoelectric mode sensors for nonuniform Euler-Bernoulli beams with rectangular cross sections [14]. Cupiał discussed a perturbation solution of the natural frequencies and mode shapes of a piezoelectric rectangular plate [15].

Daraji and Hale applied piezoelectric elements in active vibration reduction and proposed fitness and objective functions to seek optimal distribution of segmented sensors on a flexible plate [16, 17]. These researchers also developed a model for complex isotropic plate using FEM and Hamilton's principle [18].

Cazzulani et al. used the independent mode space control logics to achieve the optimal actuator and sensor placement [19]. This most popular model control logic used independently controlled modes' damping and stiffness. In this method, Ambrosio et al. proposed a negative derivative feedback strategy, which feeds velocity back to the mode and also generates a control input proportional to the compensator velocity. The feedback was able to filter out both the higher and lower uncontrolled components. In active vibration control of smart structures, the actuator and sensor placement was a key point of the control system design. Ambrosio et al. [20] also proposed an H2 norm approach to solve actuator and sensor placement. This approach was examined using a finite element model of a square plate. Piezoelectric patch actuators and acceleration sensors were mounted on the three sides of the square plate. To seek for optimal actuator and sensor placement, researchers have realized that more research effort should be made to driving forces and deformation of a piezoelectric vibrator in piezoelectric motor, micro pump, and scanner.

PZT's excitation to the vibrator is achieved through the substrate deformation caused by the piezoelectric effect. Thus, the matching relations between PZT's position and mode shape of the vibrator have great influences upon driving forces and electromechanical conversion efficiency. From the point of mode shape, this paper describes the position optimization of a PZT on a piezoelectric laminate vibrator. First, the vibrator is divided into several segments according to the cross section mutation, and then the dynamic analysis for the piezoelectric laminate structure was carried out. Then, approximate solutions of vibration modes were obtained using Rayleigh-Ritz method. These approximate solutions were compared to experimental results at their resonant frequencies. Furthermore, force coefficients at different PZT positions were discussed. These results will provide a theoretical foundation for optimizing the design of the piezoelectric laminated beam. In this paper the research objectives were to (1) conduct dynamic analysis of the piezoelectric laminated structure, (2) derive approximate solutions of vibration modes using Rayleigh-Ritz method, and (3) propose an optimization method for the design of a piezoelectric laminated beam.

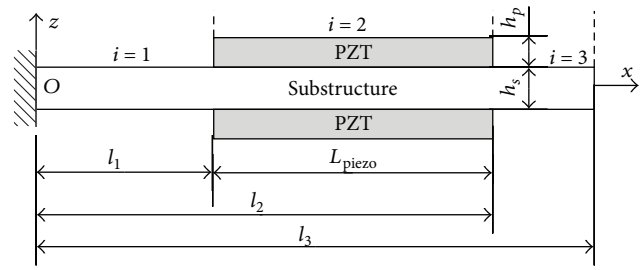

Figure 1: Bimorph piezoelectric laminated beam.

2. Dynamic Analysis on the Shape of Vibration Modes

Assume that coordinates of cross section change positions of the stepped beam of piezoelectric laminate structure in x direction are l_1, l_2, and l_3, as shown in Figure 1. The piezoelectric laminate structure was divided into several segments with equal cross section and differential equations were given for them, respectively. A characteristic matrix for the whole structure was assembled based on the continuity relationship between these segments [9].

Differential equation of the segment i is

$$(EI)_i \frac{d^4\varphi_i(x)}{dx^4} = m_i\varphi_i(x)\omega^2, \quad i = 1, 2, 3, \tag{1}$$

where $\varphi_i(x)$, $(EI)_i$, and m_i are the mode shape, bending rigidity, and mass of a unit long beam, respectively. Define

$$\beta^4 = \omega^2 \frac{m_i}{(EI)_i}. \tag{2}$$

Then (1) can be expressed as

$$\frac{d^4\varphi_i}{dx^4} = \beta_i{}^4\varphi_i(x). \tag{3}$$

The general solution for (3) is

$$\varphi_i(x) = A_i \sin(\beta_i x) + B_i \cos(\beta_i x) + C_i \sinh(\beta_i x) + D_i \cosh(\beta_i x), \tag{4}$$

where A_i, B_i, C_i, and D_i are undetermined coefficients.

For a cantilever beam, deflection and rotation angle on the left end are zero. That is to say,

$$\varphi_1(0) = \frac{d\varphi_1(0)}{dx} = 0. \tag{5}$$

In this paper, this variable cross section beam is divided into three segments. At the right end of the beam, the boundary condition is free, and both bending moment and shear force are zero. Consider

$$\frac{d\varphi_3{}^2(l_3)}{dx^2} = \frac{d\varphi_3{}^3(l_3)}{dx^3} = 0. \tag{6}$$

At the mutation sections of the beam, the deflection, rotation angle, bending moment, and shear force are continuous. That is,

$$\begin{aligned} \varphi_1(l_1) &= \varphi_2(l_1), \\ \varphi_2(l_2) &= \varphi_3(l_2) \end{aligned} \tag{7}$$

$$\begin{aligned} \frac{d\varphi_1(l_1)}{dx} &= \frac{d\varphi_2(l_1)}{dx}, \\ \frac{d\varphi_2(l_2)}{dx} &= \frac{d\varphi_3(l_2)}{dx} \end{aligned} \tag{8}$$

$$\begin{aligned} \frac{d\varphi_1{}^2(l_1)}{dx^2} &= \frac{d\varphi_2{}^2(l_1)}{dx^2}, \\ \frac{d\varphi_2{}^2(l_2)}{dx^2} &= \frac{d\varphi_3{}^2(l_2)}{dx^2} \end{aligned} \tag{9}$$

$$\begin{aligned} \frac{d\varphi_1{}^3(l_1)}{dx^3} &= \frac{d\varphi_2{}^3(l_1)}{dx^3}, \\ \frac{d\varphi_2{}^3(l_2)}{dx^3} &= \frac{d\varphi_3{}^3(l_2)}{dx^3}. \end{aligned} \tag{10}$$

The characteristic equation of the system is obtained by substituting (5)~(10) into (4). Obviously, β_i $(i = 1, 2, 3)$ is a function of the whole beam's natural frequency ω. β_i can be expressed as

$$\beta_i = \beta\alpha_i, \tag{11}$$

where $\beta = [\omega^2(m_1/(EI)_1)]^{1/4}$ and $\alpha_i = [(EI)_1 m_i/m_1(EI)_i]^{1/4}$.

The characteristic equation can also be expressed in the form of a matrix:

$$[\mathbf{J}_{12\times12} \quad \mathbf{P}_{12\times1}] = 0, \tag{12}$$

where $\mathbf{J}$ is a characteristic matrix and $\mathbf{P}$ is a feature vector which means a coefficient vector of mode shape. Consider

$$\mathbf{P} = [A_1, B_1, C_1, D_1, A_2, B_2, C_2, D_2, A_3, B_3, C_3, D_3]^T_{1\times12}. \tag{13}$$

$\mathbf{J}$ consists of three parts, as shown in (14). The first part **J1** and the third part **J3** represent the boundary conditions at the positions $x = 0$ and $x = l_3$, respectively. Part **J2** represents the continuous relationship between these segments at the mutation sections. Consider

$$\mathbf{J} = \begin{bmatrix} \mathbf{J1} \\ \mathbf{J2} \\ \mathbf{J3} \end{bmatrix}_{12\times12}, \tag{14}$$

where **J1** and **J3** are 2×12 order matrices and **J2** is an 8×12 order matrix.

The determinant of $\mathbf{J}$ is zero since the feature vector $\mathbf{P}$ has a nonzero solution. Consider

$$|\mathbf{J}_{12\times12}| = 0. \tag{15}$$

Analytical expression for ω is obtained by solving (15), and then the coefficients of mode function in (4) can be solved. It is difficult to get a nonzero solution since the equation is a higher-order transcendental equation after being unfolded. In practice, the equation is often approximately solved by making some reasonable simplifications.

3. Approximate Solution of the Mode Shape

The essence for solving mode shape is to obtain the real vibrational track of the beam under a certain order mode shape. According to Hamilton's principle, the real motion's variation for Hamilton's processing object equals zero:

$$\delta H = \delta \int_{t_1}^{t_2} L_{ag}(q, \dot{q}, t) \cdot dt = 0, \tag{16}$$

where δ is a variational symbol, H is Hamilton's magnitude, and L_{ag} is a Lagrange function defined as $L_{ag} = T_K - U$, where T_K is system kinetic energy, U is potential energy, and q is generalized coordinates. Hamilton's principle gives a way to find a true movement from all possible movements and it is generally applicable in mechanics. It has become a basic principle in mechanics field.

Rayleigh-Ritz method is a direct solution for this kind of variation problems, which extends Hamilton's principle into elastic dynamics. Its basic concept is to assume the approximate solution of a vibration mode function as follows:

$$\overline{\varphi}(x) = \sum_{j=1}^{m} \alpha_j \overline{\varphi}_j(x), \tag{17}$$

where $\overline{\varphi}_j(x)$ is defined as admissible function, α_i is undermined coefficient, and m is the item number of the admissible function sequence.

Equation (17) shows that approximate solution of a vibration mode function can be expressed by a linear combination of function sequences $\overline{\varphi}_1, \overline{\varphi}_2, \ldots, \overline{\varphi}_m$. The variational function can be converted into a function $f(\alpha_1, \alpha_2, \ldots, \alpha_m)$ of coefficients $\alpha_1, \alpha_2, \ldots, \alpha_m$. Coefficient α_j should meet the condition that the function f gets a stationary value. Consider

$$\frac{\partial f}{\partial \alpha_j} = 0 \quad (j = 1, 2, \ldots, m). \tag{18}$$

Supposing that the beam's deflection is $w(x, t)$, then the kinetic energy of the system is

$$T_K = \frac{1}{2} \int_0^{l_3} (\rho A)_x \left[\frac{\partial w(x,t)}{\partial t}\right]^2 dx. \tag{19}$$

Potential energy of the system can be written as

$$U = \frac{1}{2} \int_0^{l_3} (EI)_x \left[\frac{\partial w(x,t)}{\partial x}\right]^2 dx. \tag{20}$$

The fonctionelle of Hamilton's processing object for the beam's bending vibration can be expressed as

$$H(w) = \int_{t_1}^{t_2} (T_K - U)\, dt = \frac{1}{2} \cdot \int_{t_1}^{t_2} \int_0^{l_3} \left\{ (\rho A)_x \left[\frac{\partial w(x,t)}{\partial t} \right]^2 - (EI)_x \left[\frac{\partial w^2(x,t)}{\partial x^2} \right]^2 \right\} dx\, dt, \tag{21}$$

where $(\rho A)_x$ is the mass of a beam in unit length and $(EI)_x$ is flexural rigidity of the beam.

When the piezoelectric beam is doing a certain-order mode vibration,

$$w(x,t) = \overline{\varphi}(x) \sin(\omega t + \beta). \tag{22}$$

Substitute formula (22) into formula (21):

$$H(w) = \int_{t_1}^{t_2} (T_K - U)\, dt = \frac{1}{2} \int_{t_1}^{t_2} \int_0^{l_3} \left\{ (\rho A)_x \omega^2 \overline{\varphi}^2(x) \cdot \sin^2(\omega t + \beta) - (EI)_x \left[\overline{\varphi}''(x) \right]^2 \sin_2(\omega t + \beta) \right\} dx\, dt. \tag{23}$$

Equation (23) is the fonctionelle of the function depending on the independent variable x and t. In one cycle, which is in a range of $[0, 2\pi/\omega]$, (23) can be simplified as a fonctionelle of $\overline{\varphi}(x)$ if, integrating on t,

$$H(\overline{\varphi}) = \int_0^{l_3} \left\{ (\rho A)_x \omega^2 \overline{\varphi}^2(x) - (EI)_x \left[\overline{\varphi}''(x) \right]^2 \right\} dx. \tag{24}$$

Substitute (17) into (24); then the fonctionelle $H(\overline{\varphi})$ can be changed into a function of $(\alpha_1, \alpha_2, \ldots, \alpha_m)$. Consider

$$H(\alpha_1, \alpha_2, \ldots, \alpha_m) = \int_0^{l_3} \left\{ (\rho A)_x \omega^2 \left[\sum_{j=1}^{m} \alpha_j \overline{\varphi}_j(x) \right]^2 - (EI)_x \left[\sum_{j=1}^{m} \alpha_j \overline{\varphi}_j''(x) \right]^2 \right\} dx. \tag{25}$$

Equation (25) can also be written in a quadratic format about $\alpha_1, \alpha_2, \ldots, \alpha_m$. Consider

$$H(\alpha_1, \alpha_2, \ldots, \alpha_n) = \sum_{j=1}^{m} \sum_{k=1}^{m} \alpha_j \alpha_k \cdot \int_0^{l_3} \left[(\rho A)_x \omega^2 \overline{\varphi}_j(x) \overline{\varphi}_k(x) - (EI)_x \overline{\varphi}_j''(x) \overline{\varphi}_k''(x) \right] dx. \tag{26}$$

Defining $\widehat{m}_{jk} = \widehat{m}_{kj} = \int_0^{l_3} [(\rho A)_x \overline{\varphi}_j(x) \overline{\varphi}_k(x)]\, dx$, it is called generalized mass; defining $\widehat{k}_{jk} = \widehat{k}_{kj} = \int_0^{l_3} [(EI)_x \overline{\varphi}_j''(x) \overline{\varphi}_k''(x)]\, dx$, it is called generalized stiffness.

Equation (26) can be written in the form of a quadratic matrix:

$$H(\alpha_1, \alpha_2, \ldots, \alpha_m) = \boldsymbol{\alpha}^T (\lambda \mathbf{M} - \mathbf{K})\, \boldsymbol{\alpha}, \tag{27}$$

where

$$\begin{aligned} \boldsymbol{\alpha} &= [\alpha_1, \alpha_2, \ldots, \alpha_m]^T \\ \lambda &= \omega^2 \\ \mathbf{M} &= \left[\widehat{m}_{jk} \right], \\ \mathbf{K} &= \left[\widehat{k}_{jk} \right]. \end{aligned} \tag{28}$$

Calculate the derivatives on $\alpha_1, \alpha_2, \ldots, \alpha_m$ in formula (27), respectively, and let them be equal to zero. It can be expressed by a matrix as follows:

$$(\lambda \mathbf{M} - \mathbf{K})\, \boldsymbol{\alpha} = 0. \tag{29}$$

In order to get the nonzero solutions of $\boldsymbol{\alpha}$, its determinant of feature matrix should be equal to zero. Consider

$$|\lambda \mathbf{M} - \mathbf{K}| = 0. \tag{30}$$

Unfold the elements of matrix $\mathbf{M}$ and $\mathbf{K}$ into a segmented form:

$$\begin{aligned} \widehat{m}_{jk} &= \widehat{m}_{kj} \\ &= (\rho A)_1 \int_0^{l_1} \left[(\rho A)_x \overline{\varphi}_j(x) \overline{\varphi}_k(x) \right] dx \\ &\quad + (\rho A)_2 \int_{l_1}^{l_2} \left[\overline{\varphi}_j(x) \overline{\varphi}_k(x) \right] dx \\ &\quad + (\rho A)_3 \int_{l_2}^{l_3} \left[\overline{\varphi}_j(x) \overline{\varphi}_k(x) \right] dx \\ \widehat{k}_{kj} &= \widehat{k}_{jk} \\ &= (EI)_1 \int_0^{l_1} \left[\overline{\varphi}_j''(x) \overline{\varphi}_k''(x) \right] dx \\ &\quad + (EI)_2 \int_{l_1}^{l_2} \left[\overline{\varphi}_j''(x) \overline{\varphi}_k''(x) \right] dx \\ &\quad + (EI)_3 \int_{l_2}^{l_3} \left[\overline{\varphi}_j''(x) \overline{\varphi}_k''(x) \right] dx, \end{aligned} \tag{31}$$

where $(\rho A)_i$ and $(EI)_i$ are mass of the unit length beam and flexural rigidity of the segment i of the uniform beam ($i = 1, 2, 3$). And here

$$\begin{aligned}
(\rho A)_1 &= (\rho A)_3 = \rho_s h_s, \\
(\rho A)_2 &= 2\rho_p h_p + \rho_s h_s \\
(EI)_1 &= (EI)_3 = \frac{E_s}{12} {h_s}^3 \\
(EI)_2 &= \int_{-((1/2)h_s+h_p)}^{(1/2)h_s+h_p} z^2 dz \\
&= \int_{-(1/2)h_s}^{(1/2)h_s} z^2 dz + \int_{(1/2)h_s}^{(1/2)h_s+h_p} z^2 dz \\
&\quad + \int_{-((1/2)h_s+h_p)}^{-(1/2)h_s} z^2 dz \\
&= \frac{E_s}{12} {h_s}^3 + E_p h_p \left(\frac{{h_s}^2}{2} + h_s h_p + \frac{2}{3} {h_p}^2 \right).
\end{aligned} \tag{32}$$

Then generalized mass matrix and generalized stiffness matrix can be solved using (31).

The choice for an admissible function $\varphi_j(x)$, which is shown in (17), has significant influence on calculating accuracy and convergence rate. Ideal admissible function should not only meet the displacement boundary conditions of structural vibration but also meet the force boundary conditions. However, it is very difficult to obtain an admissible function which meets both boundary conditions. In this research, an admissible function can be acceptable as long as it meets the displacement boundary conditions. The larger the number of items m is the more accurate the approximate solution becomes. When $m \to \infty$, the approximate solution is its exact solution.

An admissible function sequence that meets the displacement boundary conditions can be assumed as

$$\underbrace{\frac{x^2}{{l_3}^2}, \frac{x^2}{{l_3}^2}\left(1 - \frac{x}{l_3}\right), \frac{x^2}{{l_3}^2}\left(1 - \frac{x}{l_3}\right)^2 \cdots}_{m}. \tag{33}$$

When $m = 1$, $m = 2$, and $m = 3$, approximate vibration mode functions are as follows:

$$\overline{\varphi}(x) = \frac{\alpha_1 x^2}{{l_3}^2} \tag{34}$$

$$\overline{\varphi}(x) = \alpha_1 \frac{x^2}{{l_3}^2} + \alpha_1 \frac{x^2}{{l_3}^2}\left(1 - \frac{x}{l_3}\right) \tag{35}$$

$$\overline{\varphi}(x) = \alpha_1 \frac{x^2}{{l_3}^2} + \alpha_1 \frac{x^2}{{l_3}^2}\left(1 - \frac{x}{l_3}\right) + \alpha_3 \frac{x^2}{{l_3}^2}\left(1 - \frac{x}{l_3}\right)^2. \tag{36}$$

4. Comparison of Theoretical and Experimental Results

In this section, the approximation method for the mode used in earlier sections was verified through vibration tests. As the first step, for the given vibrator structure, approximate function for frequency and mode shape was calculated with different numbers of items, m. The surface of the vibrator was scanned with a laser Doppler vibrometer to obtain measured value of resonant frequency. The comparison between calculated values and experimental values was executed, and causes of error were analyzed.

Table 1: Properties of the materials used.

Material	Property	Value
P81	Density (kg/m^3)	7600
	Poisson's ratio	0.32
	Young's modulus E (Pa)	1.2×10^{11}
	Piezoelectricity/$e31$ (cm^{-2})	6.04×10^{-9}
Phosphor bronze	Density (kg/m^3)	8800
	Poisson's ratio	0.33
	Young's modulus E (Pa)	1.13×10^{11}

Table 2: Dimension parameters of the vibrator (mm).

L_{piezo}	l_1	l_2	l_3	h_p	h_s
44	3	47	50	0.5	0.5

The structure of the piezoelectric laminated vibrator in the experiment is shown in Figure 1. The PZT material was P81, and substrate material was phosphor bronze. The properties of the materials and the structural parameters are shown in Tables 1 and 2. The width of the vibrator was 16 mm.

These dimensions indicate that the midpoint of the ceramic sheet was exactly coincident with the midpoint of the substrate. When the vibrator works in higher orders of vibration modes (over the third order), the amplitude was very small. Thus, only the first two modes were considered in the paper. By taking data of Tables 1 and 2 into formulas (31)-(32), elements of matrix **M** and **K** were obtained as shown in (30). Solving (30) value λ was then obtained while λ brings the information of resonant frequency ($\lambda = \omega^2$). Then, taking the value λ into (29), coefficients of mode function $\overline{\varphi}(x)$ can be solved as α_1, α_2, and α_3. The calculation results showed that only resonance frequency of the first-order bending vibration is obtained as $f_1 = 310$ Hz when $\overline{\varphi}(x)$ took a combination of admissible function with the first term in (34). When $\overline{\varphi}(x)$ took a combination of admissible function with the first two terms in (35), resonance frequencies of the first-order and second-order bending vibrations were obtained as $f_1 = 230$ Hz and $f_2 = 234$ Hz. When $\overline{\varphi}(x)$ was a combination of admissible function with the first three items in (36), resonance frequencies of the first-order and second-order bending vibrations were $f_1 = 216$ Hz and $f_2 = 1450$ Hz as shown in Table 3.

To verify the results from the method described above, a laser based noncontact instrument, Doppler vibrometer, was used to perform the scan test on the vibrator. This laser Doppler vibrometer system's components and working principle are shown in Figure 2. Operating parameters (e.g., scan range and excitation voltage) are specified on the terminal device. In this experiment, scanning frequency ranges

Table 3: Calculated and experimental values of resonant frequency under the driving voltage of 60 V.

Vibration mode	Calculated values (Hz)			Experimental values (Hz)
	$m = 1$	$m = 2$	$m = 3$	
First-order bending vibration	310	230	216	165
Second-order bending vibration		2347	1450	1420

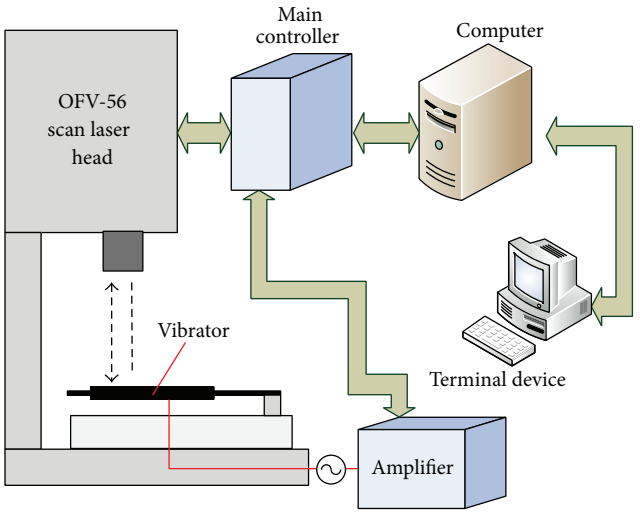

Figure 2: Laser Doppler vibration measuring for vibrator.

from 10 to 3000 Hz. Excitation voltage was 60 V, and the scanning signal was assigned by the master controller, which motivates the vibrator to work. Scanning laser head (OFV-56) sends out frequency-stabilized laser to scan the surface of the vibrator and collects the reflected light. Doppler's frequency shift signal, which is proportional to the target's velocity, is generated through interference phenomenon. After the signal is processed by a decoded controller, velocity and displacement analog values for the measured object are received. In addition, the resonant frequencies and vibration modes of the vibrator can also be obtained. All of these data will go through a high-speed A/D converter to be processed and displayed on a PC.

The calculated values and experimental results are shown in Table 3.

It can be seen from Table 3 that with just taking the first term of the admissible function into consideration ($m = 1$), the error of the theoretical value relative to the experimental value is 46.7% and that with just taking the first two terms of the admissible function sequence to form a basic function ($m = 2$), the error of the theoretical value relative to the experimental value is 28.3% for the first-order bending vibration. Similarly, it is 39.5% for the second-order bending vibration. With taking the first three terms to form a function ($m = 3$), the relative error between them is 23.6% for the first-order bending vibration and 2.1% for the second-order bending vibration. These results indicate that with more terms the approximate solution becomes more accurate. The calculated values are always greater than experimental values. These errors are mainly due to following factors.

(1) Approximation of the Admissible Function. The admissible functions only meet the displacement boundary conditions, not the force boundary conditions. The beam's ends are free in its physical model, but there are bending moment and shear force on the right end of the beam when deriving the admissible function, which is equivalent to the imposed additional constraints.

(2) Influence Caused by the External Electric Field. With the action of an electric field, the stress-strain relationship of the PZT beam can be approximately expressed using following equation:

$$\sigma_p^x = E_p^x \left(\varepsilon_p^x - \frac{d_{31} V}{h_p} \right), \tag{37}$$

where σ_p^x is the stress of PZT in x direction; E_p^x is the elastic modulus of PZT in x direction; ε_p^x is strain of PZT in x direction; d_{31} is the piezoelectric constant of PZT; V is the voltage of external electric field; and h_p is the thickness of PZT.

Equation (37) can be simplified as follows:

$$\sigma_p^x = E_{\text{effective}} \varepsilon_p^x. \tag{38}$$

Equations (37) and (38) indicate that the stress of the PZT generated from a certain strain not only is associated with the strain itself but also is related to the piezoelectric effect induced from external electric field. Under the same strain, the stress caused by PZT with external electric field became smaller than that with no external electric field. That is to say that the effective elastic modulus $E_{\text{effective}}$ is smaller than that when the external electric field is open. The higher the applied voltage in external electric field is the faster the stress decreases.

The theoretical calculation in this paper was carried out without consideration of electromechanical coupling effect from the PZT. While measuring these values at the driving voltage of 60 V, the effective elastic modulus reduces due to the action of external electric field. Thus, measured mode frequencies were less than the theoretical values.

When $m = 3$, for example, the first-order and second-order approximate vibration mode functions can be written as

$$\overline{\varphi}^{(1)}(x) = 2.5575 \frac{x^2}{l_3^2} + 1.7655 \frac{x^2}{l_3^2} \left(1 - \frac{x}{l_3} \right) + 1.9960 \frac{x^2}{l_3^2} \left(1 - \frac{x}{l_3} \right)^2$$

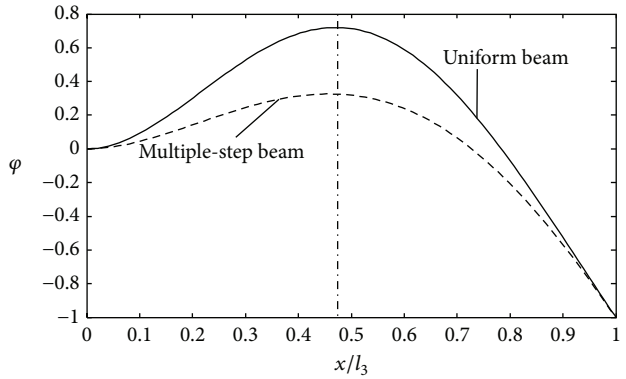

Figure 3: The second-order vibration curve of the vibrator with the PZT pasted in the center of the substrate.

$$\overline{\varphi}^{(2)}(x) = -3.5049\frac{x^2}{{l_3}^2} + 4.7098\frac{x^2}{{l_3}^2}\left(1 - \frac{x}{l_3}\right) + 30.1526\frac{x^2}{{l_3}^2}\left(1 - \frac{x}{l_3}\right)^2. \tag{39}$$

For the piezoelectric bimorph vibrator described in Figure 1, using the second-order mode can get higher electromechanical coupling effect [21]. Thus, optimized analysis of later part is aimed at the second-order mode in this study. After the length l_3 of piezoelectric beam is normalized, the curve of the second-order vibration mode shape drawn using (39) is shown in Figure 3. When comparing this curve with the vibration curve of a uniform beam, it indicates that (1) when the midpoint of the PZT beam is exactly coincident with that of the substrate the second-order vibration curve's extreme point of multiple-step beam is almost coincident with that of the uniform beam and that (2) after the vibration amplitudes on the two ends are normalized the deformation of multiple-step beam is smaller than that of uniform beam due to the influence caused by PZT.

5. Optimization of PZT Position

The second-order vibration mode of the vibrator discussed above was the case when the length L_{piezo} of PZT was nearly equal to the length of the substrate and the position of PZT was located at the center of the substrate. Next scenario to be discussed is when the length of L_{piezo} is smaller than the half wavelength of the vibration mode curve. In addition, optimal pasting position for a PZT with ideal paste condition will be discussed.

Under the ideal paste condition of the PZT, the thickness of adhesive layer between the PZT and the substrate tends to zero, and then the force exerted on the substrate by the PZT focuses on two endpoints of the ceramic sheet [10]; the relationship between the force F and the parameters of PZT is expressed as

$$\frac{F}{E_s b h_s} = \frac{\psi}{\psi + \alpha}\left[\frac{\varepsilon_B^{S+} + \varepsilon_B^{S-}}{2} + \frac{\varepsilon_B^{S+} - \varepsilon_B^{S-}}{2}\overline{x}\right] - \frac{\Lambda}{\psi + \alpha}. \tag{40}$$

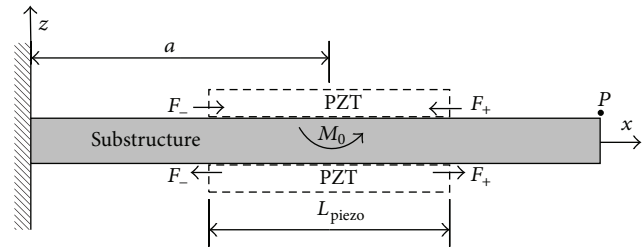

Figure 4: PZT's action on the substrate.

At the left end of the ceramic sheet, the force F_+ is expressed as

$$F_+ = E_s b h_s \frac{1}{\psi + \alpha}\varepsilon_s^{S+} - \frac{\Lambda}{\psi + \alpha}. \tag{41}$$

At the right end of the ceramic sheet, the force F_- is expressed as

$$F_- = E_s b h_s \frac{1}{\psi + \alpha}\varepsilon_s^{S-} - \frac{\Lambda}{\psi + \alpha}. \tag{42}$$

In (40), (41), and (42), F_+ and F_- are concentrated force exerted on the substrate by PZT; E_s is the elastic modulus of substrate; b is the width of PZT and h_s is the thickness of the substrate; ψ is the stiffness ratio between the substrate and PZT; ε_s^S is the surface strain of the substrate; α is a constant that reflects the strain distribution of the beam, and, for a linear Euler-Bernoulli beam, $\alpha = 6$; $\Lambda = d_{31}V/h_p$, where d_{31} is the piezoelectric constant, V is the voltage of external electric field, and h_p is the thickness of PZT.

The action force and moment of PZT on the piezoelectric vibrator are shown in Figure 4, in which a is the distance from fixed end to the midpoint of PZT, M_0 is the moment exerted from PZT to the vibrator. Generalized force Q of the piezoelectric laminated vibrator is expressed as follows:

$$\begin{aligned} Q &= \left(M_0\varphi'\right)\big|_+ - \left(M_0\varphi'\right)\big|_- \\ &= \left(Fh_s\varphi'\right)\big|_+ - \left(Fh_s\varphi'\right)\big|_-, \end{aligned} \tag{43}$$

where φ is vibration mode of the vibrator and h_s is the thickness of the substrate.

When the system is vibrating, the strain on top and bottom surfaces of the substrate is

$$\varepsilon_s^S = -\frac{h_s}{2}\frac{\partial^2 w}{\partial x^2} = -\frac{h_s}{2}\frac{\partial^2 \varphi}{\partial x^2}q = -\frac{h_s}{2}\varphi'' q. \tag{44}$$

Substituting (44) into (41) and (42), respectively, and then substituting (41) and (42) into (43), respectively, thus generalized vibrating force Q can be achieved as follows:

$$\begin{aligned} Q = &-\frac{E_s b {h_s}^3}{(\psi+\alpha)} \left[\left(\frac{h_s}{2}\varphi'' q \right)\Big|_{x=a+L_{\text{piezo}}/2} \right. \\ &\cdot \varphi'\left(a + \frac{L_{\text{piezo}}}{2}\right) - \left(\frac{h_s}{2}\varphi'' q \right)\Big|_{x=a+L_{\text{piezo}}/2} \\ &\left. \cdot \varphi'\left(a - \frac{L_{\text{piezo}}}{2}\right) \right] - E_s b {h_s}^2 \\ &\cdot \frac{\Lambda}{(\psi+\alpha)} \left[\varphi'\left(a + \frac{L_{\text{piezo}}}{2}\right) - \varphi'\left(a - \frac{L_{\text{piezo}}}{2}\right) \right]. \end{aligned} \tag{45}$$

For the first half of (45), except for q, it can be expressed as

$$\begin{aligned} &-\frac{E_s b {h_s}^3}{(\psi+\alpha)} \left[\left(\frac{h_s}{2}\varphi'' \right)\Big|_{x=a+L_{\text{piezo}}/2} \varphi'\left(a + \frac{L_{\text{piezo}}}{2}\right) \right. \\ &\left. - \left(\frac{h_s}{2}\varphi'' \right)\Big|_{x=a+L_{\text{piezo}}/2} \varphi'\left(a - \frac{L_{\text{piezo}}}{2}\right) \right] \\ &= -K_{\text{piezo}}. \end{aligned} \tag{46}$$

Then (45) can be simplified as

$$Q = -K_{\text{piezo}} q + Q_V \Lambda, \tag{47}$$

where

$$\begin{aligned} Q_V = &-E_s b {h_s}^2 \\ &\cdot \frac{\Lambda}{(\psi+\alpha)} \left[\varphi'\left(a + \frac{L_{\text{piezo}}}{2}\right) - \varphi'\left(a - \frac{L_{\text{piezo}}}{2}\right) \right]. \end{aligned} \tag{48}$$

When the piezoelectric vibrator works near the resonant frequency, it can be treated as a single degree of freedom vibration, and the vibration equation is

$$M\ddot{q} + c\dot{q} + Kq = Q. \tag{49}$$

Substituting (45) into (49), then (49) became

$$M\ddot{q} + c\dot{q} + \left(K + K_{\text{piezo}}\right) q = Q_V \frac{d_{31} V}{h_p}. \tag{50}$$

Equations (50) and (48) indicate that the mode force not only is associated with piezoelectric material properties d_{31}, voltage V of external electric field, and structural parameter h_p but also related to the position of PZT relative to the mode shapes of the vibrator. In this study, the part in brackets [] of (48) is defined as the positional force coefficient Π of PZT. Consider

$$\Pi = \varphi'\left(a + \frac{L_{\text{piezo}}}{2}\right) - \varphi'\left(a - \frac{L_{\text{piezo}}}{2}\right). \tag{51}$$

Table 4: Dimension parameters of the vibrator (mm).

L_{piezo}	l_1	l_3	h_p	h_s
15	0–35	50	0.5	0.5

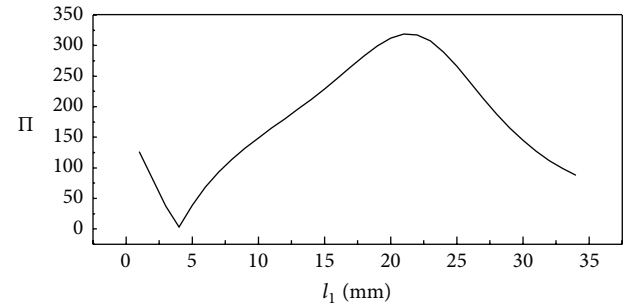

Figure 5: The variation curve of positional force coefficient Π along with the changing of PZT position on the vibrator.

According to Figures 1 and 4,

$$a = l_1 + \frac{L_{\text{piezo}}}{2}. \tag{52}$$

Then (51) can be expressed as

$$\Pi = \varphi'\left(l_1 + L_{\text{piezo}}\right) - \varphi'\left(l_1\right). \tag{53}$$

From (51) and (53) it can be seen that, with the material and geometry sizes fixed, the vibration shape curve of the piezoelectric vibrator and the positional force coefficient Π of PZT will change along with the change of PZT position. Therefore, the position of PZT on the piezoelectric vibrator will have optimal solution ever if the influence of PZT on the piezoelectric vibrator is considered.

According to the conclusion above, the first three admissible functions in sequence of the function shown in (33) were selected to study the variation of the positional force coefficient of PZT.

The structure of the vibrator is shown in Figure 1 and the parameters are given in Table 4. The width of the vibrator is 16 mm.

Through calculation, it indicates that the positional force coefficient Π of the second-order bending vibration changes along with the changing of PZT position on the vibrator, as shown in Figure 5. From the changing curve, it can be seen that when $l_1 = 4$ mm the value of Π reaches its minimum and PZT's incentive effect is lowest and when $l_1 = 21$ mm the value of Π reaches its maximum, and then the PZT's incentive effect is the best.

6. Conclusions

In this paper the researches on the influence laws of PZT position and mode shape on performance of piezoelectric vibrator are conducted. And a new optimization method for

the design of a piezoelectric laminated beam is proposed. The outcomes of this study are summarized as follows.

(1) After dividing and assembling the piezoelectric laminated vibrator with mutation sections, the dynamics equation is deduced based on the continuity boundary conditions of the vibrator.

(2) The form of vibration mode function was assumed based on the Hamilton principle and Rayleigh-Ritz method, and a sequence of admissible functions was chosen which met the displacement boundary conditions.

(3) Approximate functions of frequency and mode shape were calculated by giving different values to the item number m of the admissible function sequence, and the calculated results were compared with experimental results. It was concluded that with more items the approximate solution became more accurate. The cause of these errors was analyzed based on the selection of admissible function and the external electric field.

(4) Mode force of the piezoelectric laminated vibrator was analyzed with the action of PZT's inverse piezoelectric effect. The result indicates that mode force not only was associated with piezoelectric material properties d_{31}, voltage V of external electric field, and structural parameter but also related to the position of PZT relative to the mode shape curve of the vibrator.

Conflict of Interests

The authors declare that there is no conflict of interests regarding the publication of this paper.

Acknowledgments

This project was supported by National Natural Science Foundation of China (nos. 51475221 and 51375227), Zhejiang Provincial Natural Science Foundation of China (no. LY13E050015), and Application Type University Construction Project of Qingdao Agricultural University.

References

[1] C. S. Zhao, *Ultrasonic Motor Technology and Application*, Chinese Science Press, Beijing, China, 2007.

[2] R. R. Ramos, J. A. O. Hernandez, J. B. Castillero, and F. J. Sabina, "Electromechanical properties of laminated piezoelectric composites," *Mechanics of Composite Materials*, vol. 32, no. 3, pp. 286–291, 1996.

[3] P. Dash and B. N. Singh, "Nonlinear free vibration of piezoelectric laminated composite plate," *Finite Elements in Analysis and Design*, vol. 45, no. 10, pp. 686–694, 2009.

[4] J. A. Otero, R. Rodríguez-Ramos, G. Monsivais, and R. Pérez-Alvarez, "Dynamical behavior of a layered piezocomposite using the asymptotic homogenization method," *Mechanics of Materials*, vol. 37, no. 1, pp. 33–44, 2005.

[5] Y. Q. Huang, X. Y. Zhao, and S. X. Chen, "Rayleigh-Ritz method in elastic dynamics," *Journal of Hebei Institute of Technology*, vol. 18, no. 2, pp. 62–66, 1996.

[6] H. Zhu, *Research on Key Techniques of Traveling Wave Type and Rod Shape Ultrasonic Motor*, Nanjing University of Aeronautics and Astronautics, Nanjing, China, 2006.

[7] M. A. Koplow, A. Bhattacharyya, and B. P. Mann, "Closed form solutions for the dynamic response of Euler-Bernoulli beams with step changes in cross section," *Journal of Sound and Vibration*, vol. 295, no. 1-2, pp. 214–225, 2006.

[8] A. M. Sadri, J. R. Wright, and R. J. Wynne, "Modelling and optimal placement of piezoelectric actuators in isotropic plates using genetic algorithms," *Smart Materials and Structures*, vol. 8, no. 4, pp. 490–498, 1999.

[9] S. Bashash, A. Salehi-Khojin, and N. Jalili, "Forced vibration analysis of flexible Euler-Bernoulli beams with geometrical discontinuities," in *Proceedings of the American Control Conference (ACC '08)*, pp. 4029–4034, IEEE, Seattle, Wash, USA, June 2008.

[10] E. F. Crawley and J. de Luis, "Use of piezoelectric actuators as elements of intelligent structures," *AIAA Journal*, vol. 25, no. 10, pp. 1373–1385, 1987.

[11] J. T. Ren and J. S. Jiang, "Wave mode characteristics on piezoelectric stepped beam," *Journal of Mechanics*, vol. 36, no. 5, pp. 540–548, 2004.

[12] Y. S. Cho, Y. E. Pak, C. S. Han, and S. K. Ha, "Five-port equivalent electric circuit of piezoelectric bimorph beam," *Sensors and Actuators A: Physical*, vol. 84, no. 1, pp. 140–148, 2000.

[13] Y. Xu and D. Zhou, "Two-dimensional analysis of simply supported piezoelectric beams with variable thickness," *Applied Mathematical Modelling*, vol. 35, no. 9, pp. 4458–4472, 2011.

[14] Q. Mao, "Design of piezoelectric mode sensor for non-uniform Euler–Bernoulli beams with rectangular cross-section by using differential transformation method," *Mechanical Systems and Signal Processing*, vol. 33, pp. 142–154, 2012.

[15] P. Cupiał, "Three-dimensional perturbation solution of the natural vibrations of piezoelectric rectangular plates," *Journal of Sound and Vibration*, vol. 35, no. 10, pp. 143–160, 2015.

[16] A. H. Daraji and J. M. Hale, "Reduction of structural weight, costs and complexity of a control system in the active vibration reduction of flexible structures," *Smart Materials and Structures*, vol. 23, no. 9, Article ID 095013, 2014.

[17] A. H. Daraji and J. M. Hale, "Active vibration reduction of a flexible structure bonded with optimised piezoelectric pairs using half and quarter chromosomes in genetic algorithms," *Journal of Physics: Conference Series*, vol. 382, no. 1, Article ID 012039, 2012.

[18] A. H. Daraji and J. M. Hale, "Active vibration reduction by optimally placed sensors and actuators with application to stiffened plates by beams," *Smart Materials and Structures*, vol. 23, no. 11, Article ID 115018, 2014.

[19] G. Cazzulani, F. Resta, F. Ripamonti, and R. Zanzi, "Negative derivative feedback for vibration control of flexible structures," *Smart Materials and Structures*, vol. 21, no. 7, Article ID 075024, 2012.

[20] P. Ambrosio, F. Resta, and F. Ripamonti, "An H_2 norm approach for the actuator and sensor placement in vibration control of a smart structure," *Smart Materials and Structures*, vol. 21, no. 12, Article ID 125016, 2012.

[21] X. Q. Hu, J. H. Zhang, Y. Huang et al., "Bionic valveless piezoelectric pump," *Journal of Vibration, Measurement & Diagnosis*, supplement 1, pp. 132–135, 2012.